Forecasting Research

Forecasting Research Division
Technical Report no. 52

Balanced Surface Pressure and Temperature Increments derived from Wind Increments in the AC Assimilation Scheme.

by

P.L. Andrews and R.S. Bell

June 1993

Meteorological Office
London Road
Bracknell
Berkshire
RG12 2SZ
United Kingdom

Forecasting Research Division
Technical Report No. 52

Balanced Surface Pressure and Temperature Increments derived from Wind Increments in the AC Assimilation Scheme.

by P.L. Andrews and R.S. Bell

June 1993

Forecasting Research Division
Meteorological Office
London Road
Bracknell
Berkshire, England

Note :This paper has not been published. Permission to quote from it must be obtained from an Assistant Director of the above Met Office Division

1. Introduction

A long standing goal of the analysis correction assimilation scheme is to achieve well balanced increment fields. This is to keep the assimilation near the slow manifold, thus reducing the gravity wave noise in the analyzed fields and improving their accuracy. The balance steps also provide an approximation to multivariate analysis in the AC scheme. To this end the operational AC scheme already contains code to produce hydrostatically balanced potential temperature increments from surface pressure increments and to produce geostrophically balanced wind increments from potential temperature increments (including those derived from surface pressure increments). In this report, we describe a further balance step (WINDBAL), in which balancing surface pressure and potential temperature increments are derived from the nondivergent part of the wind increments. The theoretical basis for WINDBAL is discussed in section 2 and an *ad-hoc* approach to the scaling factors applied is given in section 3. The results of a trial using the extra balance step are discussed in section 4.

2. Theory

The problem may be broken down into two parts. First we calculate geopotential increments from the wind increment fields, and second we calculate surface pressure and potential temperature increments from these geopotential increments. In obtaining expressions for these quantities the assumption has been made that the increments are small enough to be considered linear perturbations to the background fields.

Generating the geopotential increments, $\Delta\phi$, from the wind increments, $\Delta\underline{v}$, is a straight forward process. Streamfunction increments, $\Delta\psi$, are derived from the wind increments:-

$$\Delta\psi = \nabla^{-2}[\hat{k} \cdot Curl(\Delta\underline{v})] \qquad (1)$$

A balance equation is then used to derive the geopotential increments. In this case the linear balance equation is used, hence:-

$$\Delta\phi = \nabla^{-2}[\underline{\nabla} \cdot f\underline{\nabla}(\Delta\psi)] \qquad (2)$$

where f is the Coriolis parameter.

Generating the surface pressure, ΔP_s, and potential temperature increments, $\Delta\theta$, from the geopotential increments poses somewhat more of a problem as an extra constraint is required to close the problem. Two approaches have been tried, the most successful of which is described below [the alternative method is discussed in appendix B]. The problem is shown diagrammatically in figure 1. We know the geopotential increments at each model level,

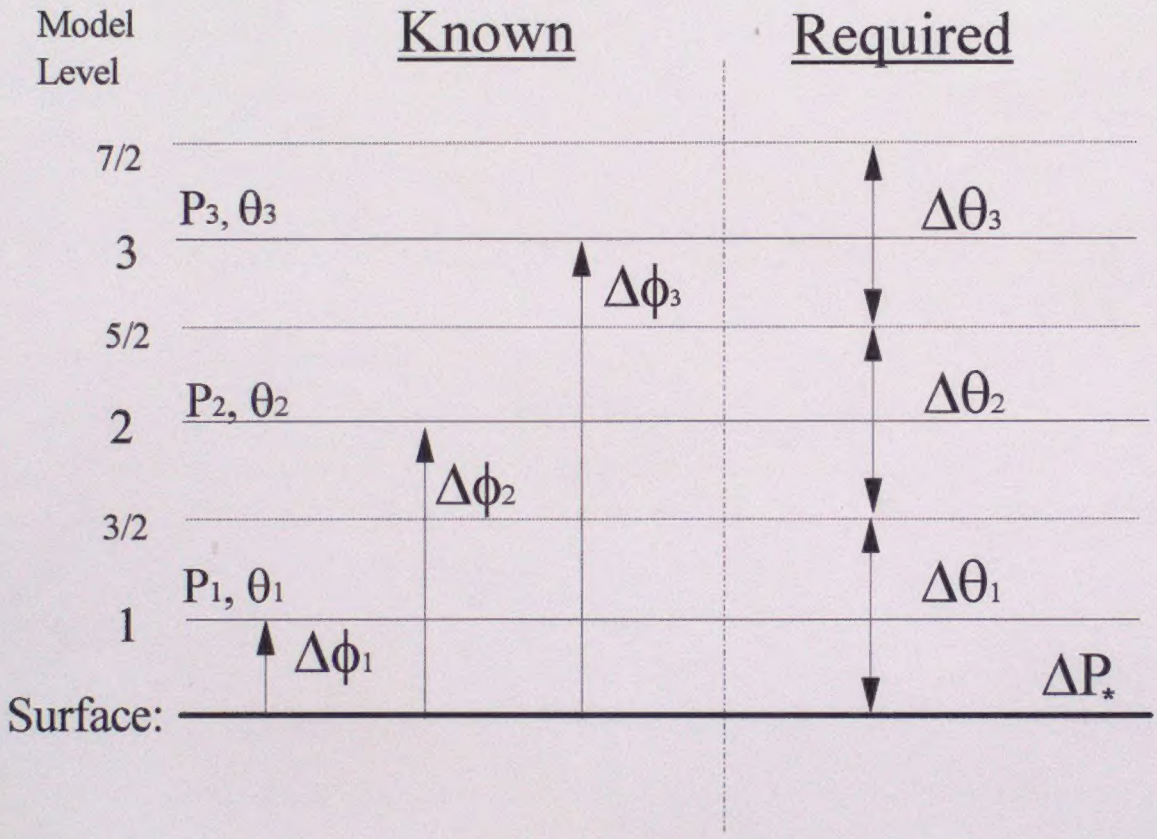

Figure 1: Diagramatic representation of the problem, showing the surface and the lowest 3 model levels (solid line) and the half levels between them (dashed lines).

together with background values, and wish to determine the potential temperature increment (defined between model half levels) at each model level, together with the surface pressure increment.

For the method described here we begin with an expression for the finite difference form of the hydrostatic equation, taken from equation 7.2a of Bell et al. 1993:

$$\Delta\theta_n = \frac{\Delta\phi_{n-\frac{1}{2}} - \Delta\phi_{n+\frac{1}{2}} + R\left[(\theta_{n+\frac{1}{2}} - \theta_n)\left(\frac{\pi B}{P}\right)_{n+\frac{1}{2}} + (\theta_n - \theta_{n-\frac{1}{2}})\left(\frac{\pi B}{P}\right)_{n-\frac{1}{2}}\right]\Delta P_*}{C_p(\pi_{n+\frac{1}{2}} - \pi_{n-\frac{1}{2}})} \qquad (3)$$

where:-

$\Delta\phi_{n+\frac{1}{2}}$	is the geopotential increment at the model half level $n+\frac{1}{2}$
$\theta_{n+\frac{1}{2}}$	is the background potential temperature at model half level $n+\frac{1}{2}$.
$P_{n+\frac{1}{2}}$	is the background pressure at model level $n+\frac{1}{2}$
$\Pi_{n+\frac{1}{2}}$	is the exner pressure at the model half level $n+\frac{1}{2}$
$B_{n+\frac{1}{2}}$	defines the boundary between model levels n & n+1
R	is the gas constant for dry air
Cp	is the specific heat at constant pressure for dry air.

Before we can solve equation 3, two things are required. First, we require the geopotential increment and the potential temperature at the half levels $n+\frac{1}{2}$, which we obtain by linear interpolation using the thickness of the layer between model levels as a weighting factor (see appendix A for details). Second, we require ΔP_*, and it is here that the extra constraint is required. Continuing with a physical approach to the problem, we note that in general the temperature of the lowest model level has little to do with the rotational wind component at that level, because of boundary layer processes. We therefore choose to impose the constraint that the temperature increment for the lowest model level be zero (note that the potential temperature increment for this model level will in general be non zero because of the contribution from ΔP_*). Now, from the definition of geopotential it is easy to see that geopotential thickness of the layer between the surface (model level = $\frac{1}{2}$) and the first model level (1) is given by:-

$$\Delta\phi_{\frac{3}{2}} = -R\ln\left(\frac{P_{\frac{3}{2}}}{P_*}\right)\Delta T_1 - R\Delta P_*\left[(T_1 - T_{\frac{3}{2}})\left(\frac{B}{P}\right)_{\frac{3}{2}} - \frac{T_1}{P_*}\right] \qquad (4)$$

Setting $\Delta T_1 = 0$ and rearranging we obtain:-

$$\Delta P_* = \frac{-\Delta\phi_{\frac{3}{2}}}{R[(T_1 - T_{\frac{3}{2}})(\frac{B}{P})_{\frac{3}{2}} - \frac{T_1}{P_*}]} \qquad (5)$$

But, $T_1 = \pi_1\theta_1$ etc. so:-

$$\Delta P_* = \frac{-\Delta\phi_{\frac{3}{2}}}{R[(\theta_1\pi_1 - \theta_{\frac{3}{2}}\pi_{\frac{3}{2}})(\frac{B}{P})_{\frac{3}{2}} - \frac{\theta_1\pi_1}{P_*}]} \qquad (6)$$

The current version of WINDBAL is an implementation of equations 1, 2, 3 and 6; together with the interpolations of appendix A and a Poisson solver (see Mawson, 1993). The Poisson solver (the only one available at present) is only able to solve Poisson's equation on the surface of a sphere, Hence WINDBAL can, at present, only be used in data assimilation of global models.

3. Correlation Coefficients

The derived potential temperature and surface pressure increments are scaled by a factor equal to the correlation coefficient between them and their true values before being used to alter the current 'background' values in the AC scheme. This is to produce a best guess at the true increments from the derived balanced increments. These correlation coefficients will be at least a function of latitude and model level and have to be determined experimentally. This was done by assuming that the difference between two nearly identical forecasts with the same validity time (one a 48 hour forecast from an initial field, the other a 6 hour assimilation followed by a 42 hour forecast starting from the same initial field) can be taken as the true increments. The true wind increments were then supplied to WINDBAL together with background values. The WINDBAL derived increments were then compared with their true values and the correlation coefficients calculated in 5° latitude bands (see figure 2). Empirical functions were then chosen to approximate these correlations. In WINDBAL the correlation function is represented as the product of a latitudinally varying correlation coefficient and a model level dependent scaling.

The form of the latitudinal correlation function is taken to be:-

Latitude	Correlation Coefficient
90° to 60° North	C_{NH}
60° to 0° North	C_{NH} * Sin (1.5 * |latitude|)
0° to 60° South	C_{SH} * Sin (1.5 * |latitude|)
60° to 90° South	C_{SH}

where: C_{NH} and C_{SH} are constants for the Northern & Southern hemispheres with current values of 0.7 and 0.8 respectively.

Figure 2: Correlation Coefficients

as a function of latitude

for model levels 4 to 15 inclusive

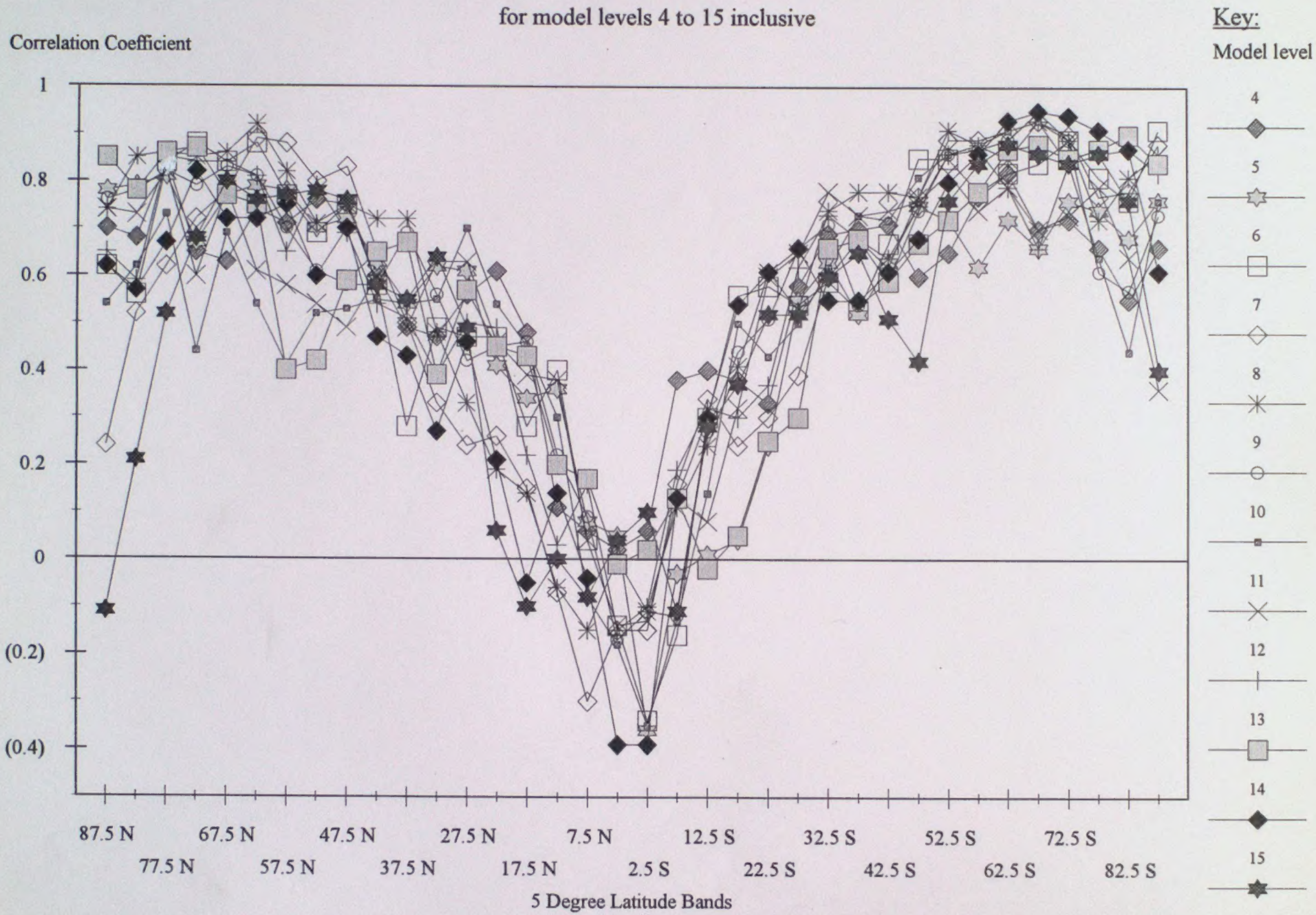

The vertical variation of this function is modeled as:-

Model Level	Scaling Factor
1 to (n-1) and (m+1) to top	0.0
n and m	0.333
(n+1) and (m-1)	0.666
(n+2) to (m-2)	1.0

where: n and m are the lower and upper bounds of non-zero vertical scaling factor (currently set as 3 and 17 in this trial of the 19 level operational global model). In the trial this scaling was not applied to the increments derived from surface winds.

An additional option, allowing these correlations to be scaled down by a further factor of 0.5 over land points, was included after preliminary tests showed a degradation in performance (as measured by short period forecast verification against radiosondes). It was considered possible that the increments fields were noisier over land where model surfaces could depart well away from the horizontal. It was also thought that increments based on the radiosonde data, which for the most part consists of coincident wind and temperature reports, would not benefit as much from the use of balancing increments as other observation types.

Note that these empirical functions are only based on one set of data. Further, that data is rather noisy - as can be seen in figures 2, 3 & 4. Clearly this situation is not ideal, and more situations need to be looked at (different synoptic situations; different lengths of forecast for determining true increments; and different seasons). In view of the noisiness of the data, however, it may well be that we can do little better than the forms assumed here.

4. Results

A global trial of 'WINDBAL' was conducted from 29th March 1993 through to the 12th April 1993. It followed the usual format established by parallel trial runs, a global data assimilation cycle plus a main 12GMT assimilation and forecast to 5 days. The verification also followed the usual format, namely an observation processing database (OPD) was generated from the data assimilation cycle giving departures from analysis and background for all observation types; and a 24 hourly verification against SYNOPs and radiosondes of the 12GMT forecast meaned over the standard verification areas (North Atlantic sector- area 2, and three latitude bands - areas 200, 300 and 400 for 90°-30°N, 30°N-30°S and 30°-90°S respectively)

After the trial was completed, it was discovered that a recent change to the operational model to improve stability (by doubling the time smoothing coefficient) had been inadvertently omitted from the parallel run. A quick check of the impact of this omission was made by rerunning the last forecast twice with the smaller and larger values of the time smoothing coefficient. The verification of this run was via the assimilation diagnostics package. It showed virtually no impact on scores from the change to the time smoothing coefficient. Typical differences in rms scores at both T+72 and T+120 were of order 0.25%, with only a very slight tendency for lower scores at T+120 when the higher value of the coefficient

was used. This one comparison is probably sufficient to confirm the validity of the parallel run.

4.1 OPD comparison

This comparison is designed to assess the performance of the data assimilation cycle by examining the fit of observations to the 6 hour forecast.

4.1.1 Surface data

The rms surface pressure observation minus background (o-b) difference showed the operational run to be 0.01hPa lower than the trial for ships in the tropics and northern hemisphere and for land synops in the northern hemisphere. Elsewhere results were identical.

The rms vector wind (o-b) difference for surface ships showed the trial to have a closer fit in the southern hemisphere (by 1.3% or 0.14 knots). Overall the results were identical elsewhere, although there was a slight indication that improvements at lower speeds were negated by degradations at higher speeds.

Taking these two results together, we can say that at the surface the impact was marginally positive in the southern hemisphere and negligible elsewhere.

4.1.2 Single level upper winds

For aircraft data (in the pressure range 100-400hPa) we see a 1.6% reduction in rms vector wind difference (rmsvwe o-b) in the trial southern hemisphere results. Outside the southern hemisphere the improvement is a more modest 0.7%. There is some indication that the very lightest winds (≤5 knots) are not fitted as well. The tables 1 and 2 below give global results in terms of mean speed difference and rms vector wind difference for selected wind speed bands and a contingency table showing the frequency distributions as a function of the same wind speed categories.

speed	trial mean (o-b)	oper mean (o-b)	trial rmsvwe	oper rmsvwe
0-5	-0.96	-1.04	6.24	6.20
5-40	-0.34	-0.36	11.88	11.90
40-80	1.32	1.44	12.98	13.10
80-120	3.56	3.72	15.46	15.58
120-160	4.76	4.96	17.22	17.32
>160	6.96	6.86	15.54	15.68
all	1.16	1.22	13.12	13.20

Table 1: Airep mean speed and rms vector wind differences from trial and operational backgrounds (units: knots, area: global).

Speed	Obs frequency	Trial frequency	Oper frequency
0-5	1.77%	1.18%	1.22%
5-40	34.07%	35.98%	36.13%
40-80	44.23%	45.02%	45.00%
80-120	16.28%	14.92%	14.79%
120-160	3.38%	2.74%	2.70%
>160	0.27%	0.16%	0.16%

Table 2: Frequency distribution of both Airep observations and model backgrounds as a function of wind speed.

The contingency table (binning observation speed against model speed) shows that the model contains fewer of the lightest winds: this is not the correct signal according to the observations. In the other categories the trial contingency table shows an improving signal with fewer model winds in the 5-40 knots band and more in the 80-120 knots and 120-160 knots bands. It has to be said that the model results are closer to each other than they are to the observations, although given that there were 129000 observations in the period, some confidence can be attached to the trend.

The fit of the backgrounds to cloud track winds gives a similar signal to that shown in the aircraft results. At both low and high levels the rms vector wind difference is 2-3% lower in the trial southern hemisphere and 0.5% lower in the tropics. In the northern hemisphere there is no change at lower levels but a 1% increase at upper levels (although data volumes are

much smaller than for aircraft reports).

4.1.3 Radiosondes

For radiosondes, the tables below show temperature and vector wind differences for the trial and operational runs for a selection of standard levels meaned over three latitude bands.

At T+6, the comparison of fit to backgrounds for temperatures, (table 3), shows a poorer trial performance at low levels and a better performance at higher levels. For winds, (table 4), we see a clear impact; the northern hemisphere is better at all levels, whilst the southern hemisphere is worse at 700hPa and above, which is in contradiction to the results for aircraft reports. In all scores the differences, whether for better or worse, are less than 1%.

Observation-analysis differences are also available from the OPD. These show a closer fit at analysis time in the trial for both winds and temperatures at nearly all levels. The only exception is at 700hPa where the temperature is marginally worse. (Note that the 850hPa (o-a) results were unavailable). The improvement of the trial over the operational control is greater at analysis time than at T+6, although it is still quite modest. The figures are not illustrated as these details are also available from the forecast verification package which is discussed in the next section.

	850hPa	700hPa	500hPa	250hPa	100hPa
NH-TRIAL	1.54	1.24	1.17	1.62	1.62
NH- OPER	1.53	1.23	1.17	1.64	1.62
TR-TRIAL	1.53	1.40	1.24	1.53	2.60
TR-OPER	1.53	1.39	1.25	1.54	2.61
SH-TRIAL	2.31	1.61	1.49	2.02	1.64
SH-OPER	2.23	1.58	1.49	2.03	1.63

Table 3: Radiosonde temperature differences from Background for both trial and operational runs for each of 3 latitude bands (units: Kelvin)

	850hPa	700hPa	500hPa	250hPa	100hPa
NH -TRIAL	8.43	8.11	9.28	11.39	8.42
NH-OPER	8.46	8.16	9.31	11.49	8.51
TR-TRIAL	8.91	9.60	10.10	14.04	13.84
TR-OPER	8.90	9.65	10.16	14.11	13.82
SH-TRIAL	12.93	12.54	14.57	17.60	12.12
SH-OPER	12.99	12.51	14.48	17.53	12.04

Table 4: Radiosonde vector wind difference from Background for both trial and operational runs for each of 3 latitude bands (unit: knots).

4.2 Forecast verification

It is clear from tables 3 and 4 that the differences between trial and control are rather modest. For clarity, the forecast verification scores are presented as a percentage change in rms error (defined as 100%*[oper. score - trial score]/oper. score, therefore negative represents a poorer trial performance). The results are presented for each verification area at 850hPa, 500hPa and 250hPa for height, temperature and wind plus surface pressure at daily forecast periods out to 5 days.

	T+0	T+24	T+48	T+72	T+96	T+120
850hPa height	-0.2	-1.5	-2.0	-3.4	-2.3	-3.3
500hPa height	-0.1	-0.4	-1.5	-3.0	-2.7	-2.5
250hPa height	-0.4	-1.3	-2.1	-2.7	-2.1	-2.9
850hPa temp	-1.0	1.0	-0.4	1.2	0.1	-0.9
500hPa temp	0.3	0.7	-1.6	-2.4	-2.3	-3.2
250hPa temp	1.8	1.8	0.0	-0.3	-0.3	-1.5
850hPa wind	0.4	-0.1	-0.5	-1.8	-0.8	-1.7
500hPa wind	1.8	0.1	0.1	-1.4	-0.9	-1.3
250hPa wind	0.8	0.9	-0.2	-1.3	-1.1	-2.2
pmsl	-1.6	-1.2	-1.5	-1.5	2.2	-3.9

Table 5: % change in rms score for Area 200 (poleward of 30°N) (see text for details).

If there is any signal identifiable from these relatively small and inconsistent differences, it can be briefly stated to be a very slight negative impact in the northern hemisphere. The upper wind and temperature rms scores are 1-2% lower in the trial at T+0 and T+24 and comparable at T+48. However height, low level temperature and pmsl results slightly favour the operational version at those times. Beyond T+48, the operational scores are lower by some 2-3%.

Tables 6 and 7 give the same results for the tropics and southern hemisphere. In the tropics, the results show a marginal improvement in the trial. (16 scores in Table 6 are greater than 1 with only 3 scores less than -1). In the southern hemisphere, the trend is also for a general improvement in scores of the trial run compared with the operational run. The exception to this is, as in the northern hemisphere, the 850hPa height and temperature and the surface pressure fields at T+0. However the improvement in upper level scores is sufficient o compensate for this and all trial results except 850hPa temperatures show an improvement at T+48 and T+72. Beyond T+72, trial heights are worse but other scores still show an improvement.

	T+0	T+24	T+48	T+72	T+96	T+120
850hPa height	-0.4	0.3	-1.0	-0.2	1.4	2.8
500hPa height	-0.2	1.3	0.2	0.9	1.6	-1.1
250hPa height	1.3	1.2	0.8	1.1	2.1	1.0
850hPa temp	0.1	0.0	1.6	0.1	0.8	-2.0
500hPa temp	0.5	-0.6	1.6	0.7	0.8	4.2
250hPa temp	-0.3	1.6	1.0	-0.5	0.5	-0.4
850hPa wind	0.0	-0.1	0.5	-0.7	-0.5	0.7
500hPa wind	0.2	0.4	0.6	0.7	-0.1	-0.4
250hPa wind	0.6	0.3	0.5	1.2	-0.4	0.5
pmsl	-0.2	0.5	-0.5	-0.7	0.3	2.9

Table 6: % change in rms score for Area 300 (30°N - 30°S) (see text for details).

	T+0	T+24	T+48	T+72	T+96	T+120
850hPa height	-4.1	-1.4	2.3	3.8	-5.1	-0.5
500hPa height	2.9	-2.4	2.8	3.1	-4.9	-1.4
250hPa height	3.2	0.4	2.0	2.8	-1.1	-6.1
850hPa temp	-1.6	-1.7	-1.8	-1.0	-1.0	-1.7
500hPa temp	-0.8	5.2	3.6	2.7	5.0	-9.6
250hPa temp	0.4	3.7	3.7	2.3	-2.0	-4.1
850hPa wind	3.6	1.4	0.1	6.0	3.0	4.7
500hPa wind	1.9	1.7	1.8	0.7	-2.3	0.3
250hPa wind	1.9	1.5	2.9	3.3	3.2	3.1
pmsl	-2.5	1.4	2.0	2.7	3.6	2.5

Table 7: % change in rms score for Area 400 (poleward of 30°S) (see text for details).

As further confirmation of the forecast differences at the longer forecast periods, the verification results against analyses were examined. These results (not shown) gave a similar

signal to the verification against observations. One important difference was in the low level temperature results in the short range forecasts, where the deterioration in trial runs was clearer. This was particularly marked in the 'Area 2' (North Atlantic) results where the 850hPa temperature rms differences were 12% greater in the trial.

4.3 Impact on Balance

The final assimilation cycle of the experiment was examined in more detail to determine what if any impact on the balance could be detected. The global rms pressure tendency and global rms divergence from a trial run were compared with comparable operational figures. This gives some indication of the change in gravity wave activity, resulting from the revised balance constraints in the assimilation. The relative values of ageostrophic and geostrophic winds were also considered.

	Trial	Operational	% difference
Global rms pressure tendency (hPa/hr)	0.54	0.58	-7.7
Global rms divergence (level 10)	0.72E-5	0.74E-5	-2.7
N. Atlantic 250hPa mean geostrophic wind speed	21.80	21.65	+0.7
N. Atlantic 250hPa mean ageostrophic wind speed	5.49	5.54	-0.9
N. Atlantic 250hPa mean wind speed	20.60	20.51	+0.4

Table 8: Comparison of balance measures.

The reductions in rms pressure tendency and rms divergence are very encouraging results and confirm that the new balance constraint has had some positive affect on the gravity wave activity. A reduction in the ageostrophic wind speed and a greater degree of geostrophic balance is also as desired.

4.4 Subjective impression of forecast impact

Given the rather inconclusive nature of the objective scores, a full subjective assessment of the trial has not been done.

A brief examination of T+0, 24 and 48 hour wind fields over the North Atlantic suggests that the trial is giving marginally greater strength in the jet core, which is beneficial.

The differences in the T+120 pmsl forecasts over the same area are sometimes substantial, but usually these differences are dwarfed by the difference of either forecast from the truth.

5. Conclusions

We have clearly achieved our aim of providing better balanced analyses and by so doing, improving the fit to data. The poorer fit to temperature data below 700hPa in the early stages of the forecast is the only disappointing aspect of the short period forecasts and this seems likely to be a primary cause of the small deterioration in the other fields at longer forecast ranges.

The correlations determined in section 3 identified potential problems at the lower levels and it seems from the trial results that these problems are greater than expected. Our ad-hoc solution to the problem closure also involves the lowest levels. Further tuning runs are planned to address this problem. Possible solutions might be to avoid using the derived temperature increments form both the surface and upper air wind analysis below level 6. The inclusion of derived increments in regions where observed increments are present from a data source which is sufficiently dense and accurate to give reliable increment fields may also be undesirable. Our rather arbitrary scaling over land points was an attempt to minimize the impact on fit to radiosonde temperatures, but perhaps a more elegant solution to this problem could be found.

The improved balance might allow us to reduce the level of divergence damping in the assimilation cycle. The level of divergence in the assimilation cycle is some 10-20% below the values from later in the forecast. A level dependence to the damping coefficient is worth considering.

It is also worth noting that the operational assimilation includes geostrophic wind increments with the same weight at all levels below the tropopause. No experiments have been done to measure their impact in the lowest levels where one might imagine geostrophic constraints should be weaker.

The cost of the new option is about 20 secs per 6 hour global assimilation.

References

R.S. Bell, A.C. Lorenc, B. Macpherson, R. Swinbank and P. Andrews, 1993, 'The Analysis Correction data assimilation scheme - version 4', *Unified Model Doc. Paper No. 30*

Mawson M., 1993, ' Solution of Poisson's equation on the sphere using Fourier transforms', *Unified Model Doc. Paper No. 14*

Appendix A: Interpolation Algorithms

The method adopted in WINDBAL requires the interpolation of some variables from levels to half levels etc. The equations used are presented here:-

$$\Delta\phi_{n+\frac{1}{2}} = \frac{\theta_n(\pi_n - \pi_{n+\frac{1}{2}})\Delta\phi_{n+1} + \theta_{n+1}(\pi_{n+\frac{1}{2}} - \pi_{n+1})\Delta\phi_n}{\theta_n(\pi_n - \pi_{n+\frac{1}{2}}) + \theta_{n+1}(\pi_{n+\frac{1}{2}} - \pi_{n+1})} \qquad \textbf{(A1)}$$

$$\theta_{n+\frac{1}{2}} = \frac{\theta_n\theta_{n+1}(\pi_n - \pi_{n+1})}{\theta_n(\pi_n - \pi_{n+\frac{1}{2}}) + \theta_{n+1}(\pi_{n+\frac{1}{2}} - \pi_{n+1})} \qquad \textbf{(A2)}$$

$$\pi_n = \frac{\pi_{n+\frac{1}{2}}P_{n+\frac{1}{2}} - \pi_{n-\frac{1}{2}}P_{n-\frac{1}{2}}}{(\frac{R}{C_p} + 1)(P_{n+\frac{1}{2}} - P_{n-\frac{1}{2}})} \qquad \textbf{(A3)}$$

Appendix B: The Curvature Method

An alternative method was tried for deriving the surface pressure increments (ΔP_*) and the potential temperature increments ($\Delta\theta_n$) from the geopotential increments ($\Delta\phi_n$). This method had the advantage of making no direct assumptions about the $\Delta\theta_1$ (or indeed the ΔT_1) value; and also of not having to interpolate from values held at model levels to model half levels etc. Thus, the $\Delta\phi_n$ values can be recalculated to machine accuracy from the derived $\Delta\theta_n$ and ΔP_* values.

Starting with equation 7.2b of Bell (1993 et al.) we have:-

$$\Delta\phi_1 = c_p(\pi_* - \pi_1)\Delta\theta_1 + R\theta_1\pi_*\frac{\Delta P_*}{P_*} \qquad \textbf{(B1)}$$

and

$$\Delta\phi_n = \Delta\phi_{n-1} + c_p[(\pi_{n-1} - \pi_{n-\frac{1}{2}})\Delta\theta_{n-1} + (\pi_{n-\frac{1}{2}} - \pi_n)\Delta\theta_n] + R(\theta_n - \theta_{n-1})(\frac{\pi B}{P})_{n-\frac{1}{2}}\Delta P_* \qquad \textbf{(B2)}$$

Rearranging and combining these we obtain:-

$$\Delta\theta_n = \frac{\Delta\phi_n - \Delta\phi_{n-1}}{c_p(\pi_{n-\frac{1}{2}} - \pi_n)} - \frac{(\pi_{n-1} - \pi_{n-\frac{1}{2}})}{(\pi_n - \pi_{n-\frac{1}{2}})}\Delta\theta_{n-1} - \frac{(\theta_n - \theta_{n-1})(\frac{\pi B}{P})_{n-\frac{1}{2}}(\Delta\phi_1 - c_p(\pi_* - \pi_1)\Delta\theta_1}{c_p(\pi_{n-\frac{1}{2}} - \pi_n)\theta_1\frac{\pi_*}{P_*}} \qquad \textbf{(B3)}$$

With equations B1 & B3 we have expressed both ΔP_* and $\Delta\theta_n$ in terms of $\Delta\theta_1$. Note, however, that equation B3 effectively derives $\Delta\theta_n$ from the half model layer between model half level n - ½ and model level n, whereas $\Delta\theta_n$ is defined as the potential temperature of the layer between model half levels n - ½ and n + ½. This discrepancy produces so called "2 delta eta" noise in the $\Delta\theta_n$: that is they tend to be alternately either too large or too small as n increases. This suggests a method of simultaneously removing the 2 delta eta noise and determining $\Delta\theta_1$: namely to minimize the sum of the squares of the curvature of the $\Delta\theta_n$ in the vertical by varying $\Delta\theta_1$. Code to do this was written, but the results were rather disappointing: whilst the ΔP_* values were good (& very similar to those found for the method described in the main text) the $\Delta\theta_n$ values were very poor. The reason for this quickly became clear when different values of $\Delta\theta_1$ were "plugged into" equation B3 together with fixed values for p, θ, $\Delta\phi$. The dependency of the $\Delta\theta_n$ on $\Delta\theta_1$ is small and rapidly decreases with increasing model level. Thus, the minimization procedure was producing excessively large values for $|\Delta\theta_1|$ whilst failing to remove the 2 delta eta noise. This method was therefore abandoned.

Forecasting Research Division Technical Reports

1.	ON THE TIME SAVING THAT CAN BE ACHIEVED BY THE USE OF AN OPTIMISED COURSE IN AN AREA OF VARIABLE FLOW	R.W. Lunnon A.D. Marklow September 1991
2.	Treatment of bias in satellite sea surface temperature observations	R.S.Bell August 1991
3.	FINITE DIFFERENCE METHODS	M.J.P. Cullen August 1991
4.	Representation and recognition of convective cells using an object-orientated approach	W.H. Hand 30th September 1991
5.	Sea-ice data for the operational global model.	C.P.Jones November 1991.
6.	Tuning and Performance of the Atmospheric Quality Control.	N.B. Ingleby. December 1991.
7.	More satellite sounding data - can we make good use of it?	R.S.Bell January 1992.
8.	WAM/UKMO Wind Wave model Intercomparison Summary Report	Heinz Gunther ECMWF Martin Holt UK Met Office January 1992
9.	Spin up problems of the UKMO Mesoscale Model and moisture nudging experiments	Akihide Segami JMA February 1992
10.	A comparison of 2nd generation and 3rd generation wave model physics	M.W. Holt B.J. Hall February 1992
11.	RETRIEVAL AND ASSIMILATION: SYSTEM CONSIDERATIONS	Andrew C Lorenc March 1992
12.	Detection of Precipitation by Radars in the UK Weather Radar Network	M. Kitchen P.M. Brown April 1992
13.	THE VALUE OF WIND OBSERVATIONS FOR WEATHER FORECASTING AND CLIMATE STUDIES	Andrew C Lorenc April 1992
14.	An investigation into the parameters used in the analysis scheme of the Mesoscale Model	G. Veitch B.J. Wright S.P Ballard May 1992
15.	THE VERIFICATION OF MESOSCALE MODEL FORECASTS OF LIQUID WATER CONTENT USING HELICOPTER REPORTS OVER THE NORTH SEA DURING WINTER 1991	M. Ahmed R.W Lunnon R.J. Graham May 1992

Forecasting Research Division Technical Reports

16.	Simulations of the Diurnal Evolution of Marine Stratocumulus Part I: The sensitivity of the Single Column Version of the Mesoscale Model to Changes in the . Turbulence Scheme.	S.D.Jackson S.P. Ballard May 1992
17.	Simulations of the Diurnal Evolution of Marine Stratocumulus Part II: A Comparison of Radiation Schemes Using the Single Column Version of the Mesoscale Model.	S.D.Jackson S.P. Ballard May 1992
18.	Quantifying the low level windshear aviation hazard for the UK: some research proposals	R.J. Graham R.W. Lunnon May 1992
19.	WAM/UKMO Wind Wave model Intercomparison Part 2 Running the UKMO wave model at higher resolution	M.W. Holt April 1992
20.	Sensitivity of Mesoscale Model forecasts of anticyclonic Statocumulus to the specifications of initial conditions and Boundary Layer mixing scheme.	B.J. Wright S.P. Ballard July 1992
21.	Evaluation of diffusion and gravity wave changes in the Global Forecast Model.	F. Rawlins O. Hammon 16 June 1992
22.	Background Errors for the Quality Control and Assimilation of Atmospheric Observations in the Unified Model - the situation in July 1992.	C.A. Parrett July 1992
23.	Estimation of the Mean and Standard Deviation of the Random Component of Data also Containing Non- random Errors.	B.R. Barwell July 1992
24.	Experiments in Nowcasting convective rain using an object- oriented approach.	W.H. Hand 15th August 1992
25.	Gravity Wave Speeds from the Eigenmodes of the Unified Model.	I. Roulstone 28 July 1992
26.	A re-calibration of the Wave Model	M.W. Holt August 1992
27.	Evaluation of Koistinen's method of radar range and bright band correction	A.G. Davies August 1992
28.	A Study of the Boundary Layer in the Mesoscale Unified Model	Graham Veitch August 21,1992
29.	Profiles of wind using time-sequences of absorption channel imagery from geostationary satellites: proof of concept using synthetic radiances	R.W.Lunnon September 1992
30.	AN EMPIRICAL INVESTIGATION OF THE "WATER VAPOUR TEMPERATURE LAPSE-RATE FEEDBACK" TO THE GREENHOUSE EFFECT	K.F.A. Smith R.J. Allam J.S.Foot September 1992
31.	Observation needs for operational ocean modelling	S.J. Foreman September 1992

Forecasting Research Division Technical Reports

32.	Bright band correlations for layered precipitation; the comparison of Chilbolton radar data and Hardaker model output.	A.G. Davies November 1992
33.	Progress and performance of the operational mesoscale model	S.P. Ballard
34.	Assessment of the bias of significant wave height in the Met.Office global wave model	S.J. Foreman M.W. Holt S. Kelsall
35.	STUDY OF CIRRUS CLOUD WINDS: ANALYSIS OF I.C.E DATA FINAL REPORT FOR EUMETSAT CONTRACT ITT 91/16	R.W. Lunnon D.A. Lowe J.A. Barnes I. Dharssi December 1992
36.	Revisions to the operational data assimilation-Nov.92	R.S. Bell January 1993
37.	A comparison of wind observations from a flight of the DRA(B)BAC 1-11 research aircraft over Hemsby, 11 June 1991, with observations from the Hemsby radiosonde	R.J. Graham January 1993
38.	The Moisture Observation Pre-processing System	B.J. Wright January 1993
39.	Performance of the data assimilation scheme in the operational trial of the new mesoscale model.	B. Macpherson B.J. Wright A.J. Maycock January 1993
40.	Development and performance of the new mesoscale model.	S.P. Ballard B. Robinson January 1993
41.	A PRELIMINARY ASSESSMENT OF OCEAN SURFACE FLUXES FROM UNIFIED MODEL FORECASTS	J.O.S. Alves S.J.Foreman M.W. Holt S. Kelsall S.J.Nightingale January 1993
42.	Some notes on primitive and quasi-equilibrium equations with a hybrid vertical coordinate and remarks on Hamiltonian structure.	I.Roulstone 23rd March 1993
43.	Development of the surface data assimilation scheme for the new mesoscale model	A.J. Maycock April 1993
44.	A REVIEW OF SEA ICE MODELS FOR USE IN FOAM	C.G. Sherlock April 1993
45.	Running the global wave model with shallow water depth information.	M.W. Holt April 1993
46.	An atlas of fetch-limited wave height over the North Sea	M.W. Holt May 1993

Forecasting Research Division Technical Reports

47.	VERIFICATION OF NWP MODEL WIND AND TEMPERATURE FORECASTS USING ASDAR REPORTS.	D.A. Forrester J. Human May 1993
48.	Use of Satellite data in the Operational Sea Surface Temperature Scheme.	C P Jones May 1993
49.	PARAMETRIZATION OF OPEN-OCEAN DEEP CONVECTION PART 1: THEORETICAL DESCRIPTION OF A PLUME ENSEMBLE MODEL	J.O.S ALVES MAY 1993
50.	PARAMETRIZATION OF OPEN-OCEAN DEEP CONVECTION PART 2:	J.O.S ALVES MAY 1993
51.	A CASE STUDY OF THE IMPACT OF RADIOSONDE TEMPERATURE AND WIND PROFILES ON MODEL FORECASTS OF A DEVELOPING ATLANTIC DEPRESSION	R.J. GRAHAM MAY 1993
52.	Balanced Surface Pressure and Temperature Increments derived from Wind Increments in the AC Assimilation Scheme.	P.L. Andrews R.S. Bell June 1993